COMPARISON OF DIFFERENT MATHEMATICAL MODELS ON THE ACCURACY OF THE ORTHORECTIFICATION OF ASTER IMAGERY

A. O. Ok [a] and M. Turker [b]

[a] METU, Graduate School of Natural and Applied Sciences, Geodetic and Geographic Information Techn. Prog. 06531 Ankara, Turkey - oozgun@metu.edu.tr

[b] Hacettepe University, Faculty of Engineering, Department of Geodesy and Photogrammetry, 06800, Beytepe, Ankara, Turkey - mturker@hacettepe.edu.tr

Commission I, WG I/6

KEY WORDS: **ASTER, Orthorectification Accuracy, Mathematical Models, Rigorous and Simple Models, Rational Functions**

ABSTRACT:

The accuracy assessments of the orthorectification of ASTER imagery carried out using twelve different mathematical models are presented. For performing the orthorectification, 77 ground control points (GCPs) and a digital elevation model (DEM) generated from stereo ASTER images were utilized. The mathematical models used include two rigorous and ten simple geometric models. Among the twelve models, the *Toutin's Rigorous Model* (Toutin, 2002) was the only model implemented using a commercial image analysis software. The mathematical models for the remaining eleven models were developed using Matlab 6.5.0. In order to find the effect of the number of GCPs on the accuracy of orthorectification, the ASTER image was rectified using evenly distributed 40, 50, 60, 70 and 77 GCPs. It was found that, the models *First Order 2D Polynomial*, *First Order Polynomial with Relief* and *Direct Linear Transformation* provided the highest RMS errors of 2.41, 1.81, and 1.62 pixels, respectively. The RMS errors computed for the models *Projective Transformation*, *Second Order 2D Polynomial*, and *Third Order 2D Polynomial* were 1.16, 1.15, and 0.99 pixels, respectively. The accuracies of the *Orun and Natarajan Model* (Orun and Natarajan, 1994) and *Toutin's Rigorous Model* were found to be 0.75 pixels. Likewise, the model *First Order Rational Functions* produced an accuracy of 0.73 pixels. The models *Second Order Rational Functions*, *Third Order Rational Functions*, and the *Second Order Polynomial with Relief*, which was developed in this study, provided accuracies in the order of half a pixel. It was found that the model *Second Order Rational Functions* provided the best results for the orthorectification of the ASTER images. However, the developed model *Second Order Polynomial with Relief* provides simplicity, consistency, and requires less number of GCPs when compared to the model *Second Order Rational Function*.

1. INTRODUCTION

A series of Earth observation satellites are monitoring our planet and acquiring a large number of images. The Terra satellite, a part of Earth Observing System (EOS) of NASA, was launched in December 1999 and began operations in February 2000. Table I summarizes the orbital characteristics of the Terra satellite. One of the payloads of Terra is a medium resolution Advanced Spaceborne Thermal Emission and Reflection Radiometer (ASTER) instrument. ASTER is a cooperative effort between NASA and Japan's Ministry of Economy Trade (METI), with the collaboration of scientific and industry organizations in both countries (Abrams et. al., 2003). ASTER is designed for not only to monitor the Earth with 14 bands but also to fulfill the elevation extraction requirements for potential users. It has three optical subsystems: the visible and near-infrared (VNIR) radiometer, shortwave-infrared (SWIR) radiometer and thermal-infrared (TIR) radiometer (Yamaguchi et. al., 1998).

The stereo image acquisition of ASTER is accomplished by the VNIR subsystem. The characteristics of the VNIR subsystem are shown in Table II. Two independent nadir and backward looking telescopes work together to obtain along-track stereoscopic images. The images taken from the nadir and backward looking telescopes compose the stereo nature with a base to height (B/H) ratio of about 0.6 and an intersection angle of about 27.7°. Since the two telescopes can be rotated up to 24° to provide extensive cross-track pointing capability and five day revisit capability, across-track stereo imaging with a better B/H ratio (close to 1) is also possible (Toutin, 2002).

The main objective of this study is to assess the accuracies of the orthorectification of ASTER nadir imagery using two rigorous geometric models. Then, the accuracies were evaluated using ten simple geometric models. The accuracies were calculated using different numbers of GCPs and ICPs. The objectives were met by implementing the model in a 60 x 60 km study area enclosing the city of Ankara.

Parameter	Specification
Orbital Path	Near-polar Sun-synchronous
Orbits / cycle	233
Cycle duration	16 days
Number of orbits per day	14
Altitude	705 km
Inclination	98.3 deg
Orbital Period	98.88 min
Equatorial crossing at local time	10:30 am

Table 1. The orbital characteristics of Terra satellite

Parameter	VNIR subsystem
Telescopes	Nadir and Backward
Spectral range	Green, Red, NIR for Nadir, NIR for Backward
Resolution	15 m
Along-track B/H ratio	0.6
Cross-track pointing	±24°
Coverage	60 x 60 km
Quantization	8 bits

Table 2. The characteristics of VNIR system

2. STUDY AREA AND DATA SETS

2.1 Study Area

The study area is located in central Anatolia. It covers an area of approximately 60 x 60 km and encloses the city of Ankara (Fig. 1). The other urban areas present in the area include several scattered towns. The Lakes Mogan and Eymir illustrated as 'B' in Figure 1 are situated in the central part of the area. The area also contains several randomly distributed small water bodies. A part of the eastern site illustrated as 'C' is rather mountainous. The forested areas represented as 'D' are mostly located in the southern part of the city of Ankara and in the south western part of the mountainous areas. The rest of the study area is characterized by the mixture of agricultural areas and open lands, which are represented as 'E' in Figure 1. The elevations range from approximately 700 m for the flat areas to 1900 m for the mountainous areas yielding a total relief around 1200 m. The slopes change sharply in mountainous regions approaching up to 70 degrees.

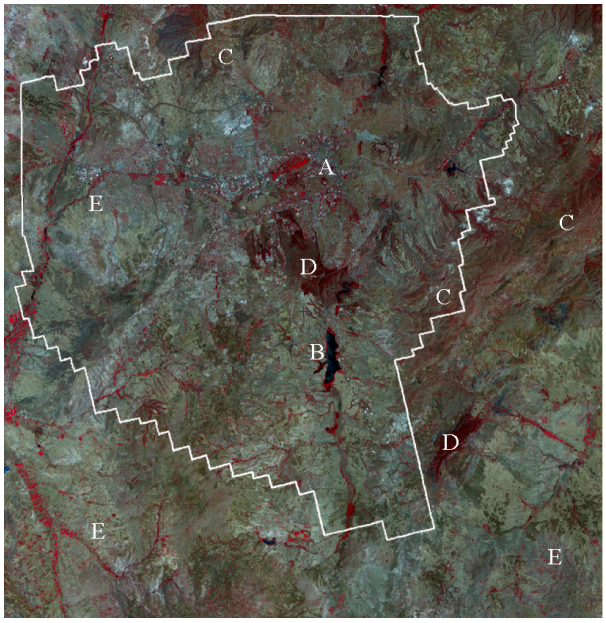

Fig. 1. The ASTER nadir image of the study site. (A) represents the city center of Ankara, (B) represents the Lake Mogan, (C) represents the mountainous sites, (D) represents the forestry areas, and (E) represents the agricultural and open lands. The vector polygon shows the coverage of the existing vector data and orthophotos.

The main reason for selecting this area to implement the models is that it contains various land-use and land-cover types that include urban, forest, water, mountainous, agriculture and open lands. The other reason is that both in the city of Ankara and in rural areas a number of roads and paths exist that can be selected as GCPs and ICPs.

2.2 Data Sets

The ASTER nadir image was acquired on July 26, 2002. The processing level of the scene was Level 1A, which is raw data format and completely free from clouds, snow and other effects, such as haze and dust. The ASTER Level-1A data consist of the image, the radiometric coefficients, the geometric coefficients and other auxiliary data without applying the coefficients to the image data to maintain the original data values (ASTER Users Guide, 2003).

The 1:5000-scale digital orthophotos covering the study area were also available to be used for selecting the Ground Control Points (GCP). The orthophotos were produced in 1999 and referred to the European ED 50 datum and the Transverse Mercator (Gauss – Krueger) projection. The pixel size of the digital orthophotos is 1 m, while the planimetric accuracy is approximately 20 cm. When collecting the GCPs, the digital orthophotos and the ASTER image were displayed simultaneously on the screen and a total of 61 GCPs were collected. The elevations of the GCPs were obtained from a DEM, which was generated from existing 1:1000-scale vector dataset, which contains the 1 m interval contour lines, the individual elevation points, road network, and valley creeks. The accuracy of the vector data is approximately 20 cm both in planimetry and elevation. Consequently, the accuracy of the GCPs collected was better than 1 m both in planimetry and elevation.

In those areas that were not covered by the orthophotos, the GCPs were collected through differential GPS (DGPS) measurements. Unfortunately, the medium resolution nature of the ASTER stereo images restricted us to select the main road intersections as the GCPs. On the other hand, due to the lack of features no suitable GCPs were found on top of the mountainous areas. Thus, a total of 16 GCPs were able to be found and their coordinates were measured on the ground using DGPS technique. With the GPS-measured control points, the total number of points increased to 77.

The DEM generated from the vector data covers about 57% of the ASTER image. Therefore, an additional DEM was generated from the stereo ASTER images using the Orthoengine module of PCI Geomatica image analysis software. The accuracy assessment of the generated DEM was performed based on the check points (CPs), slopes, and land cover types in a previous study conducted by Ok and Turker (2005). Finally, the accuracy was assessed using 2,171,664 elevation points and the overall accuracy of the DEM was computed to be 10.92 m.

3. SENSOR MODELS FOR ORTHORECTIFICATION

The raw images collected from different platforms usually contain distortions. The distortions can be classified in six main categories and be summarized as distortions due to platform variations, sensor, instrument and viewing angle errors, atmospheric effects, Earth based distortions and map

projections errors (Toutin, 2004). All these distortions must be modelled and corrected by using a specific mathematical model. Several mathematical models can be used for this purpose but the availability of the ephemeris and attitude data directly influences the model type. If the position and the attitude data of a sensor are known during image acquisition, a rigorous model can be used, threfore. Otherwise, a simple geometric model must be used in order to cope with these distortions.

3.1 Rigorous Geometric Models

3.1.1 Toutin's Model

This model uses a rigorous mathematical model developed in Canada Centre for Remote Sensing (CCRS) and reflects the physical reality of the complete viewing geometry and integrates all the distortions generated during image acquisition (Toutin and Cheng, 2002). The distortions handled by the Toutin's model include distortions due to platform, sensor, Earth, and cartographic projection. Integrating all these distortions in a mathematical model produces a set of correlated unknown parameters, which are later reduced to a set of independent uncorrelated set (Toutin and Cheng, 2002). Based on the quality of the GCPs, the accuracy of the Toutin's model was proven to be within one-third of a pixel for medium resolution VIR images, one to two pixels for high-resolution VIR images, and within one resolution cell for SAR images (Toutin and Cheng, 2002). Among the twelve models tested in this study, Toutin's model was the only one implemented using the Orthoengine module of the PCI Geomatica software.

3.1.2 Orun and Natarajan Model

A frame camera uses the collinearity equations to relate the image space and the object space. However, because the pushbroom image acquisition technique uses the line perspective geometry when acquiring the images, the collinearity conditions cannot be implemented in the same way. The mathematical model of the collinearity equations must be modified to line perspective (Novak, 1992):

$$x_a^i = x_0 - f\left[\frac{m_{11}^i(X_A - X_L^i) + m_{12}^i(Y_A - Y_L^i) + m_{13}^i(Z_A - Z_L^i)}{m_{31}^i(X_A - X_L^i) + m_{32}^i(Y_A - Y_L^i) + m_{33}^i(Z_A - Z_L^i)}\right] \quad (1)$$

$$0 = y_0 - f\left[\frac{m_{21}^i(X_A - X_L^i) + m_{22}^i(Y_A - Y_L^i) + m_{23}^i(Z_A - Z_L^i)}{m_{31}^i(X_A - X_L^i) + m_{32}^i(Y_A - Y_L^i) + m_{33}^i(Z_A - Z_L^i)}\right] \quad (2)$$

where; x^i_a is the coordinate in a scan line, orthogonal to the direction of travel. Because the images are acquired in lines, y_i dimension can be neglected and defined as zero. Another difference between the frame and pushbroom sensors is the exterior orientation parameters of the acquired images. Because a frame sensor acquires the whole image in an instantaneous of time the exterior orientation parameters of a frame camera images are fixed. On the other hand, because the pushbroom sensors acquire the images in a period of time they have different exterior orientation parameters for each scan line which makes the computations much more complicated than the frame sensor. Until now, the change of the exterior orientation parameters has been approximated by different polynomial orders of time (first, second and third order). It appears that, the quadratic polynomial formulation of the change in exterior orientation has been widely used:

$$\begin{aligned} X_L^i &= X_L + a_1 \times t_i + b_1 \times t_i^2 \qquad \omega^i = \omega_L + a_4 \times t_i + b_4 \times t_i^2 \\ Y_L^i &= Y_L + a_2 \times t_i + b_2 \times t_i^2 \qquad \varphi^i = \varphi_L + a_5 \times t_i + b_5 \times t_i^2 \\ Z_L^i &= Z_L + a_3 \times t_i + b_3 \times t_i^2 \qquad \kappa^i = \kappa_L + a_6 \times t_i + b_6 \times t_i^2 \end{aligned} \quad (3)$$

where; X^i_L, Y^i_L, Z^i_L are the exterior orientation parameters of line i, X_L, Y_L, Z_L are the positional exterior orientation parameters of the center-line of the scene, ω_L, φ_L, κ_L are the rotational exterior orientation parameters of the center-line of the scene, a_1, a_2, a_3, a_4, a_5, a_6, b_1, b_2, b_3, b_4, b_5, b_6 are the linear coefficients of the exterior orientation parameters and t_i is the time of line i. In this case, there are additional 12 unknown parameters to the regular 6 unknown parameters (X_L, Y_L, Z_L, ω_L, φ_L, κ_L) when compared to the frame sensors.

The mathematical formulations of the exterior orientation parameters look so non-problematic. However, there is a major problem which the nature of the pushbroom sensor would cause. For instance, in the case of a second order polynomial approximation for the exterior orientation parameters, 18 unknowns cannot be solved in a single estimation procedure due to the correlations between the parameters. Unlike the frame sensors, the results of the least squares estimation are unstable due to one dimensional nature of the sensor. This problem was explained and solved by Orun and Natarajan (1994). The resulting model changes the phi and kappa orientations to time independent values, while other parameters remain unchanged. As a result, 18 unknowns in the general model are reduced to 12 unknown parameters in the Orun and Natarajan model.

$$\begin{aligned} X_L^i &= X_L + a_1 \times t_i + b_1 \times t_i^2 \qquad \omega^i = \omega_L + a_4 \times t_i + b_4 \times t_i^2 \\ Y_L^i &= Y_L + a_2 \times t_i + b_2 \times t_i^2 \qquad \varphi^i = \varphi_L \\ Z_L^i &= Z_L + a_3 \times t_i + b_3 \times t_i^2 \qquad \kappa^i = \kappa_L \end{aligned} \quad (4)$$

3.2 Simple Geometric Models

A simple geometric model usually involves mathematical models, which are easier to understand and do not require the knowledge of image sensor physics (Toutin, 2004). These systems neither use nor require information related to the sensor, platform, the Earth, and do not reflect the geometry of the distortions. In this respect, simple geometric models require simple mathematical models to relate the image space and the object space.

Until now, a number of different simple geometric models with different orders have been introduced. These include the 2D Polynomial Models, the 3D Polynomial Models, the Rational Functions, the Projective Transformation, and Direct Linear Transformation.

3.2.1 2D Polynomial Models

In this method, the relation between the image space and the object space is formed using the planimetric coordinates of the GCPs only. The general mathematical formulation of a 2D polynomial function can be expressed as (Toutin, 2004):

$$P_{2D}(x, y) = \sum_{i=0}^{m} \sum_{j=0}^{n} a_{ij} X^i Y^j \quad (5)$$

where; X and Y are the planimetric coordinates of the GCPs, i and j are the increment values, m and n determine the order of

the polynomial model, generally between one and five, and a_{ij} are the polynomial coefficients to be determined by the least squares approach. Because, 2D Polynomial models do not take into account the elevations of the GCPs these models can be efficiently used when the study area is relatively flat. Furthermore, in order to achieve a good accuracy, the GCPs have to be accurate, numerous, and evenly distributed across the image.

3.2.2 3D Polynomial Models

3D polynomial functions are generated by adding the elevation coordinates of the GCPs to the 2D polynomial functions using new parameters. However, because they are similar to the 2D order polynomial functions the problems of the 2D order polynomial functions are also valid for these functions except for the topography. These models still require accurate, numerous, and evenly distributed GCPs. The general form of the 3D polynomial functions can be expressed as (Toutin, 2004):

$$P_{3D}(x,y) = \sum_{i=0}^{m}\sum_{j=0}^{n}\sum_{k=0}^{p} a_{ijk} X^i Y^j Z^k \tag{6}$$

where; *X, Y and Z* are the coordinates of the GCPs, *i, j* and *k* are the increament values, *m, n* and *p* determines the order of the polynomial model, generally between one and three (Tao and Hu, 2001), and a_{ij} are the polynomial coefficients to be determined by the least squares adjustment.

Special forms of the 3D polynomial functions are also available. Pala and Pons (1995) have modified the first order 2D polynomial model by taking into account the relief displacement effect. They derived the 3D polynomial model for the images that are acquired from high altitude and they assumed a flat Earth model. The generated model has 4 additional unknowns for x and y, when compared to the first order polynomial model and comprises a total of 12 unknown parameters:

$$\begin{aligned} x &= a_1 + a_2X + a_3Y + a_4Z + a_5XZ + a_6YZ \\ y &= b_1 + b_2X + b_3Y + b_4Z + b_5XZ + b_6YZ \end{aligned} \tag{7}$$

In this study, the second order of the previous model was developed. Therefore, instead of using the first order polynomial model, the second order polynomial functions were used as the starting point. The resulting special form of the polynomial functions double the unknowns with respect to the first order special function and can be expressed as:

$$\begin{aligned} x &= a_1 + a_2X + a_3Y + a_4X^2 + a_5Y^2 + a_6XY + a_7Z + a_8XZ + a_9YZ \\ &\quad + a_{10}X^2Z + a_{11}Y^2Z + a_{12}XYZ \\ y &= b_1 + b_2X + b_3Y + b_4X^2 + b_5Y^2 + b_6XY + b_7Z + b_8XZ + b_9YZ \\ &\quad + b_{10}X^2Z + b_{11}Y^2Z + b_{12}XYZ \end{aligned} \tag{8}$$

Since these special polynomials were generated by taking into account the terrain relief effect, they are called "Polynomial Model with Relief" in this study.

3.2.3 Rational Functions

Rational Functions perform transformations between the image and the object spaces through a ratio of 3D polynomials. The general form of the rational functions can be written as (Toutin, 2004):

$$R_{3D}(x,y) = \frac{\sum_{i=0}^{m}\sum_{j=0}^{n}\sum_{p=0}^{p} a_{ijk} X^i Y^j Z^k}{\sum_{i=0}^{m}\sum_{j=0}^{n}\sum_{p=0}^{p} b_{ijk} X^i Y^j Z^k} \tag{9}$$

where; a_{ijk} are the polynomial coefficients that are called rational functions. One important difference of the rational functions is that both the image coordinates (x,y) and the object coordinates (X, Y, Z) are normalized to fit the range from -1 to +1 to minimize the errors during the computations and to improve the numerical stability of the equations.

In this study, the rational functions coefficients are estimated from the available GCPs. Therefore, this is also called the terrain dependent method. One major disadvantage is that the increase of the Rational function coefficients (RFCs) also increases the possibility of the correlation between the RFCs and can make the least squares estimation instable.

3.2.4 Projective Transformation

The projective transformation describes the relationship between the two planes (Novak, 1992). It is the basic fractional model which can relate the image space and the object space. It integrates only the planimetric coordinates as the 2D polynomial model. The projective transformation is also called eight parameter transformation because the total of unknowns of the model are eight:

$$x = \frac{a_1X + a_2Y + a_3}{c_1X + c_2Y + 1} \quad y = \frac{b_1X + b_2Y + b_3}{c_1X + c_2Y + 1} \tag{10}$$

where; a_1, a_2, a_3, b_1, b_2, b_3, c_1, and c_2 are the eight unknown parameters of the functions.

3.2.5 Direct Linear Transformation (DLT)

The DLT models the transformation between the image pixel coordinate system and the object space coordinate system as a linear function (Mikhail et. al., 2001). This model has been widely used in close range photogrammetry and the model is often used to derive the approximate initial values of the unknown parameters for the collinearity equations. DLT has three additional unknowns when compared to the Projective Transformation:

$$x = \frac{a_1X + a_2Y + a_3Z + a_4}{c_1X + c_2Y + c_3Z + 1} \quad y = \frac{b_1X + b_2Y + b_3Z + b_4}{c_1X + c_2Y + c_3Z + 1} \tag{11}$$

where; a_1, a_2, a_3, a_4, b_1, b_2, b_3, b_4, c_1, c_2, and c_3 are the linear orientation parameters between two dimensional image space and three dimensional object space.

4. THE RESULTS

In this study, the models used for the orthorectification process include (1) *Toutin's model*, (2) *Orun and Natarajan model*, (3-5) *2D polynomials (first, second, and third degrees)*, (6-8) *Rational Functions (first, second, and third degrees)*, (9-10) *Polynomial Model with Relief (first and second degrees)*, (11) *Projective Transformation (1st degree)*, and (12) *Direct Linear*

Transformation (DLT) (1st degree) models. Among the 12 models, the *Toutin's model* was the only one implemented using a commercial software. The mathematical models for the remaining 11 models were developed using Matlab 6.5.0.

First, of the available 77 points, evenly distributed 40 were selected as the GCPs and the remaining 37 were used as independent check points (ICP) for assessing the accuracy of the generated orthorectified images. In order to find the effect of the number of GCPs on the accuracy of the orthorectification, the nadir image was rectified using the evenly distributed 50, 60, 70 and 77 GCPs.

The performances of the rigorous and the simple geometric models under different evenly distributed GCP and ICP combinations are sumarized in Table 3 and Table 4, respectively. All errors are given and evaluated in the image space.

Rigorous Models	**GCPs / ICPs**	**GCP RSME (pixel)**	**ICP RSME (pixel)**
Toutin's	40 / 37	0.81	0.76
	50 / 27	0.80	0.70
	60 / 17	0.80	0.62
	70 / 7	0.78	0.49
	77 / 0	0.75	-
Orun and Natarajan	40 / 37	0.81	0.75
	50 / 27	0.79	0.73
	60 / 17	0.79	0.63
	70 / 7	0.77	0.53
	77 / 0	0.75	-

Table 3. The results of the rigorous models for different number of evenly distributed GCPs.

Of these models, the *First Order Polynomial Function* provided the RMS error over two pixels for both GCPs and ICPs. Therefore, it can be stated that the results of the *First Order Polynomial Function* were the worst among 12 models and therefore, definitely it should not be used. The RMS error values of the *First Order Polynomial Function with Relief* and the *DLT models* were higher than 1.5 pixels. Although, for these models, the accuracies of the ICPs were better than the accuracies of the GCPs, it can be stated that these models have limited orthorectification capabilities and therefore, they should not be used either.

The RMS error values were found to be slightly higher than one pixel for both the GCPs and ICPs when the *Second Order Polynomial* and the *Projective Transformation models* were used. For these models, the RMS errors of the ICPs were computed to be around one pixel. For the *Third Order Polynomial model*, the RMS error of the GCPs was one pixel. Consequently, the models *Second Order Polynomial*, *Projective Transformation*, and the *Third Order Polynomial* can be used for the orthorectification of the ASTER imagery when sub pixel accuracy is not required and if the models that provide higher accuracy are not readily available.

The accuracies of the two rigorous models the *Orun and Natarajan model* and the *Toutin's model* were found to be the same. For these two models, the trends for the GCPs and ICPs were almost indistinguishable. The lowest RMS error value was computed to be 0.75 pixels. The model *First Order Rational Functions* produced similar RMS error values when compared to the rigorous models. The trend for the GCPs and ICPs were similar to the rigorous models as well. Consequently, the results of the orthorectification using the *Orun and Natarajan model*, the *Toutin's model* and the *First Order Rational Functions* were found to be good for both the GCPs and ICPs.

Simple Models	**GCPs / ICPs**	**First-Order**		**Second-Order**		**Third-Order**	
		GCP RSME (pixel)	**ICP RSME (pixel)**	**GCP RSME (pixel)**	**ICP RSME (pixel)**	**GCP RSME (pixel)**	**ICP RSME (pixel)**
2D Polynomial	40 / 37	2.75	2.17	1.23	1.14	0.99	1.11
	50 / 27	2.65	2.02	1.21	1.08	1.04	0.96
	60 / 17	2.56	1.91	1.20	1.02	1.04	0.85
	70 / 7	2.48	1.74	1.17	1.00	1.01	0.81
	77 / 0	2.41	-	1.15	-	0.99	-
Polynomial with Relief	40 / 37	1.92	1.76	0.61	0.78	-	
	50 / 27	1.88	1.74	0.64	0.69		
	60 / 17	1.84	1.79	0.66	0.59		
	70 / 7	1.88	0.94	0.65	0.58		
	77 / 0	1.81	-	0.64	-		
Rational Functions	40 / 37	0.77	0.75	0.42	0.73	0.26	0.84
	50 / 27	0.76	0.73	0.50	0.60	0.33	0.85
	60 / 17	0.77	0.64	0.52	0.55	0.38	0.59
	70 / 7	0.75	0.56	0.51	0.63	0.39	0.72
	77 / 0	0.73	-	0.51	-	0.40	-
Projective Transformation	40 / 37	1.25	1.13	-		-	
	50 / 27	1.22	1.09				
	60 / 17	1.20	1.03				
	70 / 7	1.18	1.00				
	77 / 0	1.16	-				
DLT	40 / 37	1.76	1.61	-		-	
	50 / 27	1.74	1.49				
	60 / 17	1.68	1.51				
	70 / 7	1.67	1.08				
	77 / 0	1.62	-				

Table 4. The RMS errors of the orthorectified ASTER imagery using simple geometric models

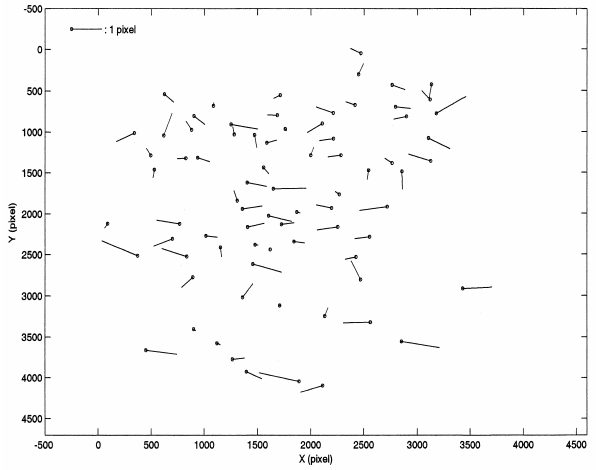

Fig. 2. The error vectors of the 77 GCPs for the *Second Order Polynomial with Relief* model developed in this study.

The RMS errors of the models *Second and Third Order Rational Functions* were approximately half a pixel when the assessments were carried out based on the GCPs. Furthermore, the model *Third Order Rational Functions* provided the results as accurate as a quarter of a pixel. However, it was observed that the accuracies of the ICPs were affected conversely in the *Third Order Rational Functions* model. Although the *Third Order Rational Functions* model fits the GCPs very well, it distorted the ICPs a little more when compared with the *Second Order Rational Functions* model. Therefore, the *Second Order Rational Functions* model is said to be better than the *Third Order Rational Functions* model. The *Second Order Polynomial with Relief* model produced RMS errors close to the *Second and Third Order Rational Functions* models. For the *Second Order Polynomial with Relief* model, the RMS errors of ICPs were computed to be better than the *Third Order Rational Functions* model and were almost equal to the errors of the *Second Order Rational Functions* model. The error vector results of the 77 GCPs for the *Second Order Polynomial with Relief* model are illustrated in Figure 2.

5. CONCLUSIONS

In this study, the orthorectification accuracies of the ASTER imagery conducted using two rigorous and ten simple geometric models were presented. Based on the results, it can be stated that the *Second Order Rational Functions* model provided the lowest RMS errors for the orthorectification of the ASTER imagery. However, the *Second Order Rational Functions* suffers from the correlated parameters within the model. Because of the correlations between several parameters, the implementation of the *Second Order Rational Functions* model can only be performed if the least squares adjustment solution is modified. Therefore, although the accuracy of the *Second Order Polynomial with Relief* model was a little bit worse than the accuracy of the *Second Order Rational Functions* model, it can be stated that the *Second Order Polynomial with Relief* model appears to be superior to the *Second Order Rational Functions* model in terms of simplicity and consistency. Furthermore, the minimum number of GCPs required for the *Second Order Polynomial with Relief* model was significantly lower than the *Second Order Rational Functions* model. Therefore, the authors claim that the *Second Order Polynomial with Relief* model developed in this study can be efficiently used for the orthorectification of the ASTER imagery.

REFERENCES

Abrams, M., Hook, S., and Ramachandran, B., 2003. ASTER User Handbook Version 2.

ASTER Users Guide Part II, ver. 4, (2003).

Mikhail, E. M., Bethel, J. S., and McGlone, J. C., 2001. Introduction to Modern Photogrammetry.

Novak, K., (1992), Rectification of Digital Imagery, Photogrammetric Engineering and Remote Sensing, Vol. 58, No. 3, pp. 339-344.

Ok, A. O., Turker, M., 2005. DEM Generation and Accuracy Assessment from Stereo ASTER Imagery. Proceedings of the 2nd International Conference on Recent Advances in Space Technologies, pp. 523-528, Istanbul, Turkey.

Orun, A. B., and Natarajan, K., 1994. A Modified Bundle Adjustment Software for SPOT Imagery and Photography: Tradeoff, Photogrammetric Engineering and Remote Sensing, Vol. 60, No. 12, pp. 1431-1437.

Pala, V., and Pons, X., 1995. Incorporation of Relief in Polynomial-Based Geometric Corrections, Photogrammetric Engineering and Remote Sensing, Vol. 61, No. 7, pp. 935-944.

Tao, C. V., and Hu, Y., 2001. Use of the Rational Function Model for Image Rectification, Canadian Journal of Remote Sensing, pp. 593-602.

Toutin, T., 2002. Three Dimensional Topographic Mapping with ASTER Stereo Data in Rugged Topography, IEEE Transactions on Geoscience and Remote Sensing, Vol. 40, No. 10, pp. 2241-2247.

Toutin, T., and Cheng, P., 2002. Comparison of Automated Digital Elevation Model Extraction Results using Along-track ASTER and Across-track SPOT images, SPIE Journal, Optical Engineering, Vol. 41, No. 9, pp. 2102-2106.

Toutin, T., 2004. Review Article: Geometric Processing of Remote Sensing Images: Models, Algorithms and Methods, International Journal of Remote Sensing, Vol. 25, No. 10, pp. 1893-1924.

Yamaguchi, Y., Kahle, A. B., Tsu, H., Kawakami, T., and Pniel, M., 1998. Overview of Advanced Spaceborne Thermal Emission and Reflection Radiometer (ASTER), IEEE Transactions on Geoscience and Remote Sensing, Vol. 36, No. 4, pp. 1062-1071.